Available online at www.sciencedirect.com
ScienceDirect
Cement & Concrete Composites 30 (2008) 524–534
Cement & Concrete Composites
www.elsevier.com/locate/cemconcomp

Behavior of corrosion-damaged RC columns wrapped with FRP under combined flexural and axial loading

Tamer El Maaddawy *

UAE-University, Al-Ain, Abu Dhabi, P.O. Box 17555, United Arab Emirates

Received 25 May 2007; received in revised form 15 January 2008; accepted 15 January 2008
Available online 26 January 2008

Abstract

This paper presents the results of a research program aimed at investigating the effectiveness of carbon fiber-reinforced polymers (CFRP) to upgrade corrosion-damaged eccentrically loaded reinforced concrete (RC) columns. A total of 16 square RC columns with end corbels were constructed. Test specimen had an overall length of 1200 mm whereas each end corbel had a cross section of 250×250 mm and a length of 350 mm. The specimen in the test region was 125×125 mm having longitudinal steel ratio of 1.9%. The damaged specimens were exposed to 30 days of accelerated corrosion that corresponded to a steel mass loss of about 4.25%. The main test parameters were the CFRP repair scheme (no wrapping, full-wrapping, and partial-wrapping) and the eccentricity-to-section height (e/h) ratio (0.3, 0.43, 0.57, and 0.86). The strength of the damaged columns fully wrapped with CFRP was up to 40% higher than that of the control undamaged columns. The strength gain was inversely proportional to the eccentricity ratio. Partial CFRP-wrapping was 8% less effective than full CFRP-wrapping at nominal e/h of 0.3. At higher e/h values, the confinement level had a negligible effect on the columns' strength. An analytical model was then proposed to predict the columns' strength under eccentric loading. A comparative analysis between predicted and experimental results demonstrated the model's accuracy and reliability.

Keywords: Corrosion; Concrete; Flexural; Axial; Eccentric; Columns; CFRP

1. Introduction

The warm marine climate along with the saline ground water in the Middle East result in major corrosion problems in reinforced concrete (RC) structures. A large number of existing RC infrastructures in Europe, North America and many other developed countries are also suffering from active corrosion because of the use of de-icing salts. Corrosion damage is usually observed as rust stains and minute cracking over the concrete surface running parallel to the underlying steel bars. This is because of the volume increase associated with the formation of corrosion products. At time of corrosion cracking, the reduction in the steel cross sectional area is insignificant [1–3]. However, if repairs are not taken at this early stage, the corrosion will continue, leading to concrete delamination and spalling rendering exposed steel reinforcement. This would accelerate the corrosion rate, further reduce the steel cross sectional area to a level that might cause a safety hazard.

Externally bonded fiber-reinforced polymers (FRP) have emerged as a promising rehabilitation system to upgrade deficient RC components. A considerable amount of research confirmed the ability of FRP system to upgrade corrosion-damaged RC elements under pure flexural loading [4–6]. The effectiveness of FRP system to increase the structural capacity of corroded RC columns under concentric loading has been reported in numerous studies [7–9]. In field conditions, RC columns are often, however, exposed to eccentric loading. The efficacy of FRP to improve the seismic resistance, ductility and energy absorption capacity of RC piers and bridge columns is well documented in the literature [10–12]. Few researchers have examined the behavior of undamaged RC columns repaired with FRP

* Tel.: +971 50 8310915; fax: +971 3 7623154.
E-mail address: tamer.maaddawy@uaeu.ac.ae

0958-9465/$ - see front matter © 2008 Elsevier Ltd. All rights reserved.
doi:10.1016/j.cemconcomp.2008.01.006

under monotonically increasing eccentric loading [13–15]. FRP system was found to be less effective in increasing the structural capacity of undamaged RC columns under eccentric loading. To date, no data is available in the literature on the viability of using FRP system to upgrade corrosion-damaged RC columns when exposed to combined flexural and axial loading.

The present work is a part of an ongoing research program aimed at investigating the short and long-term performance of corrosion-damaged RC columns repaired with carbon fiber-reinforced polymers (CFRP) under eccentric loading. In this paper the viability of using CFRP system to upgrade eccentrically loaded corroded RC columns in the short-term is examined. An analytical model that can predict the strength of eccentrically loaded RC columns wrapped with FRP is proposed and verified against test results. The post-repair performance of CFRP-repaired columns under corrosive environmental conditions will be presented in another publication.

2. Experimental program

2.1. Test matrix

The test matrix is given in Table 1. The specimens were divided into four main groups, [A], [B], [C], and [D], each having four specimens. Specimens of group [A] were uncorroded–unwrapped and used as control. Specimens of groups [B], [C], and [D] were exposed to 30 days of accelerated corrosion exposure under a constant current density of 90 $\mu A/cm^2$. Following corrosion exposure, specimens of group [B] were tested to failure without repair while specimens of groups [C] and [D] were repaired with full and partial CFRP-wrapping systems, respectively, then tested to failure under various eccentric loading. The eccentricity to section height (e/h) ratios were selected so that the uncorroded–unwrapped specimens (group [A]) will have all possible modes of failure (compression, balanced, and tension modes of failure). Steel coupons were extracted from some of the specimens exposed to corrosion after conducting the structural test to failure. The steel mass loss was then measured gravimetrically according to the ASTM Standard G1-90 [16]. Thirty days of corrosion exposure corresponded to an average steel mass loss of about 4.25%.

2.2. Test specimens

A schematic for test specimen is shown in Fig. 1. Test specimen was a square RC column (125×125 mm) with end corbels each having cross sectional dimension of 250×250 mm. The overall length of the test specimen was 1200 mm, including end corbels (350 mm length each). A larger cross section could not be employed because of the limitation in the capacity of the reaction frame available in the structural laboratory at the UAE-University. The longitudinal steel reinforcement in the test region consisted of four No. 10 deformed steel bars which corresponded to a steel reinforcement ratio of about 1.9%. The ties were 6 mm diameter plain bars spaced at 125 mm on center (OC) in the middle 250 mm of the test region. To prevent any premature failure at the ends of the test region the tie spacing were reduced to 62.5 mm OC over a 125 mm length at each end. The concrete cover up to the surface of the longitudinal steel bars was 21 mm which corre-

Table 1
Test matrix

Group	Specimen[a]	Corrosion time (days)[b]	Confinement condition	Nominal e/h
[A]	NUW-e1	–	No-wrapping	0.30
	NUW-e2	–	No-wrapping	0.43
	NUW-e3	–	No-wrapping	0.57
	NUW-e4	–	No-wrapping	0.86
[B]	CUW-e1	30	No-wrapping	0.30
	CUW-e2	30	No-wrapping	0.43
	CUW-e3	30	No-wrapping	0.57
	CUW-e4	30	No-wrapping	0.86
[C]	CFW-e1	30	Full-wrapping	0.30
	CFW-e2	30	Full-wrapping	0.43
	CFW-e3	30	Full-wrapping	0.57
	CFW-e4	30	Full-wrapping	0.86
[D]	CPW-e1	30	Partial-wrapping	0.30
	CPW-e2	30	Partial-wrapping	0.43
	CPW-e3	30	Partial-wrapping	0.57
	CPW-e4	30	Partial-wrapping	0.86

[a] N and C refer to no corrosion and corrosion, respectively. UW, FW, and PW refer to unwrapped, fully wrapped, and partially wrapped specimens, respectively. e1, e2, e3, and e4 refer to nominal e/h values of 0.3, 0.43, 0.57, and 0.86, respectively.

[b] 30 days of accelerated corrosion exposure corresponded to a steel mass loss of about 4.25% (steel mass loss was measured according to the ASTM Standard [16]).

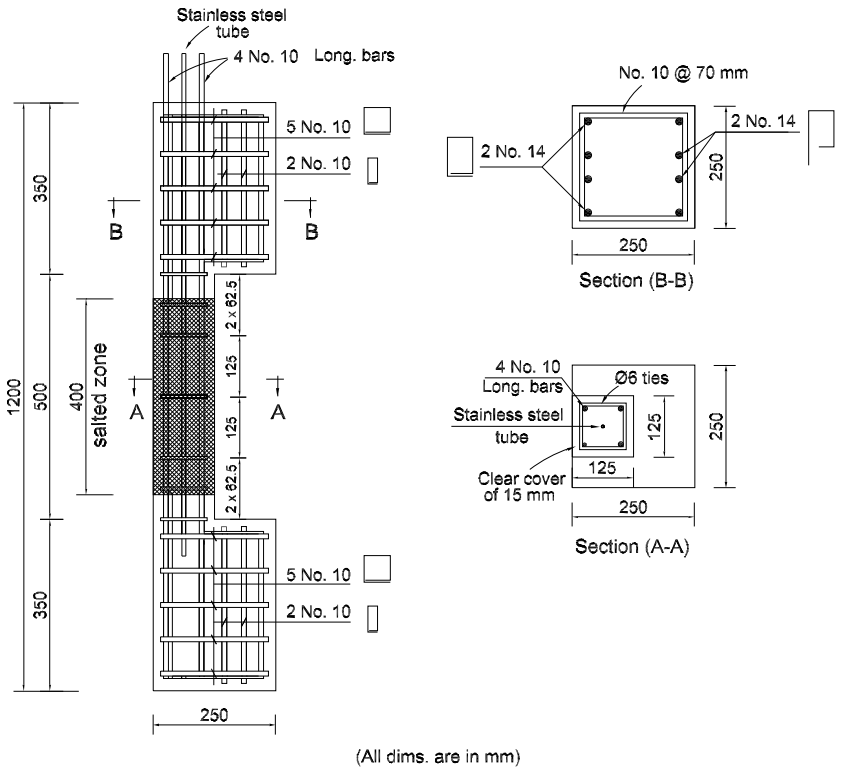

Fig. 1. Details of test specimen.

sponded to cover-to-bar diameter ratio (c/d) of about 2. A tubing stainless steel bar with inner and outer diameters of 6 and 8 mm, respectively was placed in the middle of the column to act as a cathode during the accelerated corrosion process. The longitudinal steel reinforcing bars and the stainless steel tube were extended about 100 mm out of one end of the specimen to facilitate connecting the steel and the stainless bars to an external power supply during the accelerated corrosion process. To depassify the longitudinal steel reinforcement and promote corrosion, 3% NaCl was added to the concrete mix used to cast the middle 400 mm of the column in the test region. The end corbels were designed to have flexural and shear strengths well in excess of the anticipated failure load of the column's section in the test region.

2.3. Material properties

The concrete compressive strength was on average 28.5 MPa with a corresponding standard deviation of 2.5 MPa. The longitudinal steel reinforcement was Grade 520 with yield and ultimate strengths of 550 and 725 MPa, respectively. The CFRP fabric used to repair the corrosion-damaged specimens was unidirectional with nonstructural weaves in the secondary direction to hold the fabric together. According to the data sheet provided by the manufacturer, a dry CFRP fabric has a tensile strength of 3.45 GPa, an elastic modulus of 230 GPa, and an elongation at break of 1.5% The fabric was laminated to the specimens with an epoxy resin having tensile strength of 30 MPa and an ultimate elongation of 1.5%. A cured CFRP laminate has a thickness of 0.381 mm, an average tensile strength of 894 MPa, a tensile modulus of 65.4 GPa, and an ultimate elongation of 1.33% (information was extracted from the manufacturer data sheet).

2.4. Test set-up

An impressed current technique was utilized in the present study to induce corrosion in test specimens within a reasonable time. A constant current of 75 mA that corresponded to about 90 $\mu A/cm^2$ current density was used during the accelerate corrosion process. The current was impressed on the steel reinforcing bars by means of an external DC power supply. The power supply has a current capacity of 400 mA which can be controlled in increments of 1 mA with a current accuracy of 1%. The power supply allows the application of a constant current with an automatic crossover, which changes the non-constant parameters, voltage or power, automatically to maintain the current constant. The corroded specimens were connected in series in order to ensure that the electrical current passing through all specimens was the same. The steel reinforcement bars were connected to the positive terminal of the power supply to act as an anode while the stainless steel tube was connected to the negative terminal of the power supply to act as a cathode. Fogging compressed air mist

nozzle was utilized to spray mist over the test specimens to facilitate corrosion reactions. A photo of test specimens under accelerated corrosion exposure is shown in Fig. 2.

Eventually, all test specimens were tested under monotonically increasing eccentric loading. A new set of loading plates was developed for eccentric loading application (Fig. 3). The set is composed of two parts: top plate with knife-edge and adaptor plate. Four V-notch grooves were cut through the adapter plate from above at desired locations. The test specimen was rested on another inverted set of eccentric loading plates to maintain the load eccentricity. A hydraulic Jack was used to apply monotonic load to test specimens. A calibrated load cell was placed between the Jack and the reaction frame to record the load. Two linear variable differential transducers (LVDTs) were mounted on the concrete surface in the longitudinal direction, one at compression side and one at tension side, to measure the longitudinal displacement over a 375 mm gauge length. One additional LVDT was used to measure the lateral displacement at the mid-height of the column. A photo of a test in progress is shown in Fig. 4.

2.5. CFRP repair technique

Two CFRP repair schemes were used in the present study to repair corrosion-damaged specimens (Fig. 5). In scheme I (full-wrapping), one layer of continuous CFRP laminate was wrapped around the column's section in the test region with the fibers oriented in transverse direction. In repair scheme II (partial-wrapping), one layer of CFRP strips, 65 mm wide each, having a clear spacing of 40 mm were wrapped around the column's section in the test region with the fibers oriented in transverse direction. At the ends of the test region, the strip width was increased to 125 mm to avoid premature failure at these locations. The CFRP laminates had an overlap of 50 mm in transverse direction.

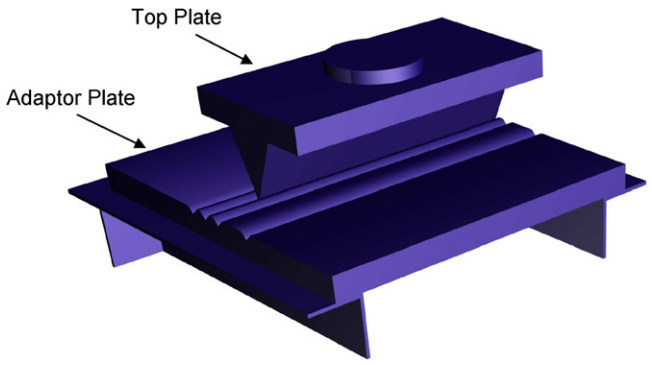

Fig. 3. Loading plates.

The CFRP repair system included surface preparation and CFRP application. A grinder was first utilized to remove any dust and loose particles from the concrete surface. The specimen's corners were rounded to a radius of about 10 mm. A high-pressure air jet was then used to clean the surface from dust or any foreign particles after the grinding process. An epoxy resin was then applied directly onto the prepared substrate using a trowel. The CFRP fabrics, pre-cut to desired dimensions, were then placed onto the resin coating and smoothed out with gloved hands. A laminating roller was utilized to work out any irregularities and expel any air pockets. Adequate pressure was applied until the resin was squeezed out between the fabric's rovings. A final sealer coat of resin was then applied onto the exposed surface. The wrapped specimens were then left at room temperature to allow curing of the bonded CFRP laminates.

3. Experimental results and discussion

3.1. Corrosion damage

The first visible corrosion crack appeared after about 4 days of accelerated corrosion exposure. During the early

Fig. 2. Accelerated corrosion exposure.

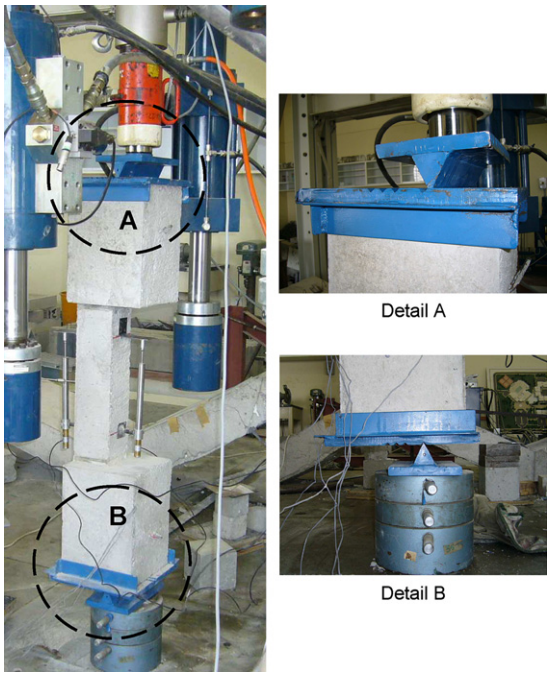

Fig. 4. A test in progress.

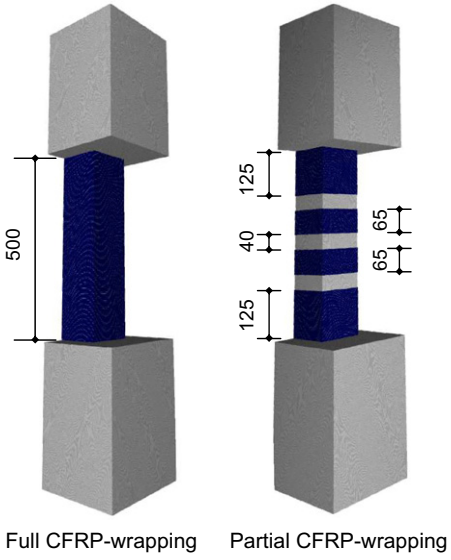

Fig. 5. CFRP repair schemes.

stages of accelerated corrosion exposure, a white line of NaCl deposit was observed around each crack. Subsequently a mixture of relatively red-black corrosion products was observed leaching out of the cracks rendering severe rust stains and concrete deterioration. At the end of the accelerated corrosion process, all corroded specimens exhibited longitudinal cracks running parallel to the steel reinforcing bars. No spalling of concrete was observed at the end of the accelerated corrosion exposure that corresponded to a steel mass loss of about 4.25%. The corrosion crack width at the end of the accelerated corrosion process was measured by a microscope that provides a magnification of 25× and a resolution of ±0.05 mm. The maximum measured corrosion crack width was in the range of 0.3–0.65 mm with an average of 0.4 mm and a corresponding standard deviation of 0.12 mm. Corrosion cracks and rust stains observed in test specimens at the end of the accelerated corrosion exposure are shown in Fig. 6.

3.2. Load carrying capacity

Compression strength results are presented in Fig. 7 and summarized in Table 2. Because of the nature of the test set-up the applied axial force was coupled with a bending moment. The total moment at mid-height reported in Table 2 consists of primary moment computed based on the initial (nominal) eccentricity and the secondary moment caused by the lateral mid-height displacement at failure. The secondary moment varied from 8% to 21% relative to the total applied moment (primary moment + secondary moment). The actual eccentricity used to calculate the actual e/h at failure was computed by dividing the total moment by the failure load. From Fig. 7, it can be seen that the strengths of the corroded-unwrapped specimens (group [B]) were almost the same as those of their counterparts from group [A] that were not corroded. This indicates that 4.25% steel mass loss has no noticeable effect on the load carrying capacity of eccentrically loaded RC columns. It is evident that CFRP-wrapping system enhanced the compression strength of RC columns under eccentric loading. The strengths of the damaged columns fully wrapped with CFRP (group [C]) were 40%, 26%, 8%, and 5% higher than those of the undamaged columns (group [A]) at nominal e/h values of 0.3, 0.43, 0.57 and 0.86, respectively. The strength gain was inversely proportional to the eccentricity ratio because higher eccentricity ratio resulted in a smaller compressed concrete area at failure thereby reducing the effect of confinement provided by the CFRP. At nominal e/h value of 0.3, the strength of the partially wrapped specimen was about 8% lower than that of the fully wrapped specimen. No significant variation in strength between the fully and partially wrapped specimens was observed at higher e/h values.

3.3. Load–lateral displacement curves

The load versus lateral mid-height displacement curves for specimens of groups [A] and [B] are shown in Fig. 8. As planned in the design, specimens of group [A] experienced three different modes of failure. Specimens NUW-e1 and NUW-e2 had compression mode of failure in which failure occurs suddenly by crushing of concrete at compression side without yielding of tension steel. Specimen NUW-e3 had balanced mode of failure where concrete crushing and yielding of tension steel almost occurred at the same time. Specimen NUW-e4 had tension mode of failure where yielding of tension steel preceded crushing of concrete at compression side. At e/h value of 0.57, corrosion

Fig. 6. Corrosion damage.

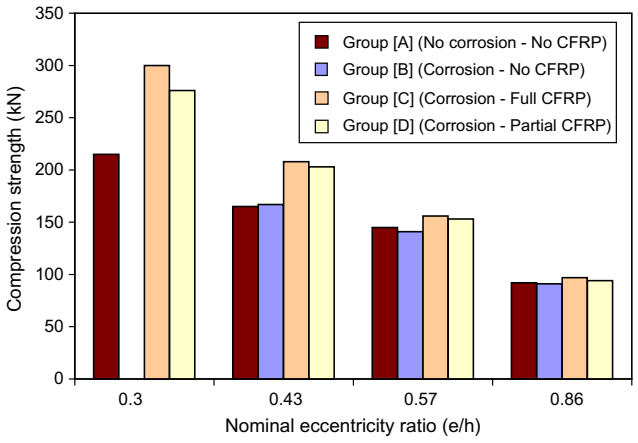

Fig. 7. Compression strength results.

of steel reinforcement changed the mode of failure from a balanced mode of failure to a tension failure mode. This is because of the reduction in the steel area caused by corrosion which allowed for yielding of tension steel prior to concrete crushing.

From Fig. 8, it can be seen that the flexural stiffness, characterized by the slope of the curve, of the corroded-unwrapped specimens (group [B]) were slightly higher than those of the uncorroded specimens (group [A]). This might be ascribed to the roughness of corrosion products that improved the bond between steel and concrete. The enhancement in bond strength at low degrees of corrosion is well documented in the literature [17]. Visual examination of concrete pieces taken from corroded specimens after conducting the structural test to failure confirmed the presence of marks from the steel reinforcing bars' ribs indicating good bond condition between steel and concrete.

Fig. 9 presents the load versus lateral mid-height displacement curves for specimens of groups [C] and [D] that were fully and partially wrapped with CFRP, respectively. The CFRP wrapped specimens experienced two modes of failure. Specimens CFW-e1 and CPW-e1 failed by rupture of CFRP in transverse direction/bursting of concrete at compression side without yielding of tension steel (compression failure). In all other wrapped specimens failure occurred by rupture of CFRP in transverse direction/bursting of concrete at compression side that was preceded by yielding of tension steel (tension failure). Various failure modes observed in the present study are shown in Fig. 10.

All partially wrapped specimens exhibited lower flexural stiffness than that of the fully wrapped specimens. This can be attributed to the lower confinement provided by the partial-wrapping relative to that provided by the full-wrapping. Yielding of tension steel, which is characterized by the change in the slope of the curve, is clearly apparent in all wrapped specimens with the exception of specimens CFW-e1 and CPW-e1 that exhibited a compression mode of failure. The yield load increased as e/h decreased. Fully wrapped specimens had slightly higher yield load than that of the partially wrapped specimens.

Table 2
Test results

Group	Specimen	Compression strength (kN)	Primary moment (kN m)	Secondary moment (kN m)	Total moment (kN m)	Actual e/h at failure
[A]	NUW-e1	215	8.06	2.04	10.10	0.376
	NUW-e2	165	8.91	1.75	10.66	0.517
	NUW-e3	145	10.30	1.49	11.79	0.650
	NUW-e4	92	9.89	0.86	10.75	0.935
[B]	CUW-e1[a]	NA	NA	NA	NA	NA
	CUW-e2	167	9.02	1.49	10.51	0.503
	CUW-e3	141	10.00	1.30	11.30	0.641
	CUW-e4	91	9.78	0.76	10.54	0.927
[C]	CFW-e1	300	11.25	3.09	14.34	0.382
	CFW-e2	208	11.23	2.08	13.31	0.512
	CFW-e3	156	11.08	1.84	12.92	0.663
	CFW-e4	97	10.43	1.03	11.46	0.945
[D]	CPW-e1	276	10.35	2.73	13.08	0.379
	CPW-e2	203	10.96	1.91	12.87	0.507
	CPW-e3	153	10.86	1.76	12.62	0.660
	CPW-e4	94	10.10	0.90	11.00	0.936

[a] Specimen was broken during handling.

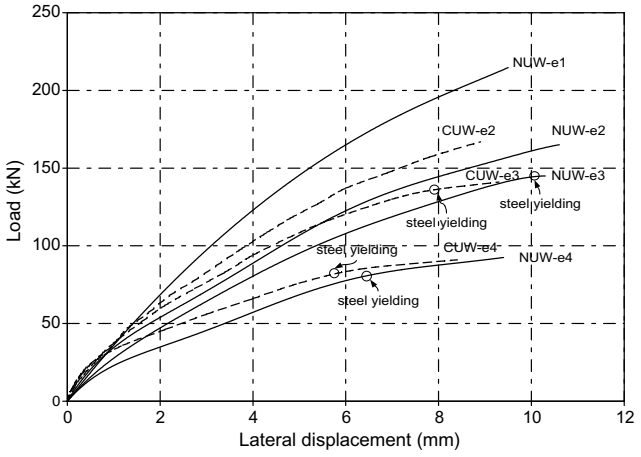

Fig. 8. Load–lateral displacement curve; groups [A] and [B].

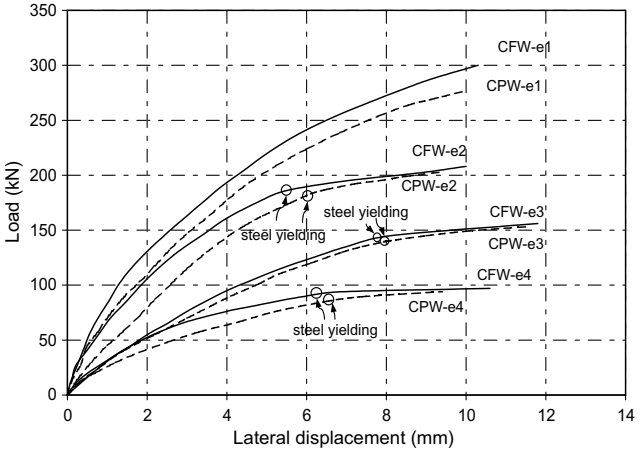

Fig. 9. Load–lateral displacement curve; groups [C] and [D].

3.4. Load–longitudinal strain relationships

The load versus longitudinal compressive concrete strain relationships for specimens of group [B] that were corroded unwrapped and specimens of group [C] that were corroded then wrapped with full CFRP system are shown in Fig. 11. The relationship for specimen NUW-e1 from group [A] is also shown in the same figure. It is evident that the wrapped specimens exhibited superior ultimate compressive strains relative to those of the unwrapped specimens. Full CFRP-wrapping system resulted in about 80% average increase in the ultimate compressive strain relative to that of the unwrapped specimens. This is because of the confinement effect provided by CFRP which increased the ultimate compressive strain of the wrapped concrete to levels higher than those of the unwrapped concrete. The load versus longitudinal compressive concrete strain relationships for specimens of groups [A] and [D] were similar to those of groups [B] and [C], respectively and hence they are not shown in Fig. 11 for clarity. However, the ultimate compressive strains of specimens of group [D] that were partially wrapped with CFRP were on average 9% lower than those of specimens of group [C] that were repaired by full CFRP-wrapping system. This is because partial CFRP wrapping provides less confinement than full CFRP-wrapping.

4. Analytical modeling

An analytical model is proposed to verify test results and to predict the strength of eccentrically loaded corroded RC columns wrapped with CFRP. The model is based on

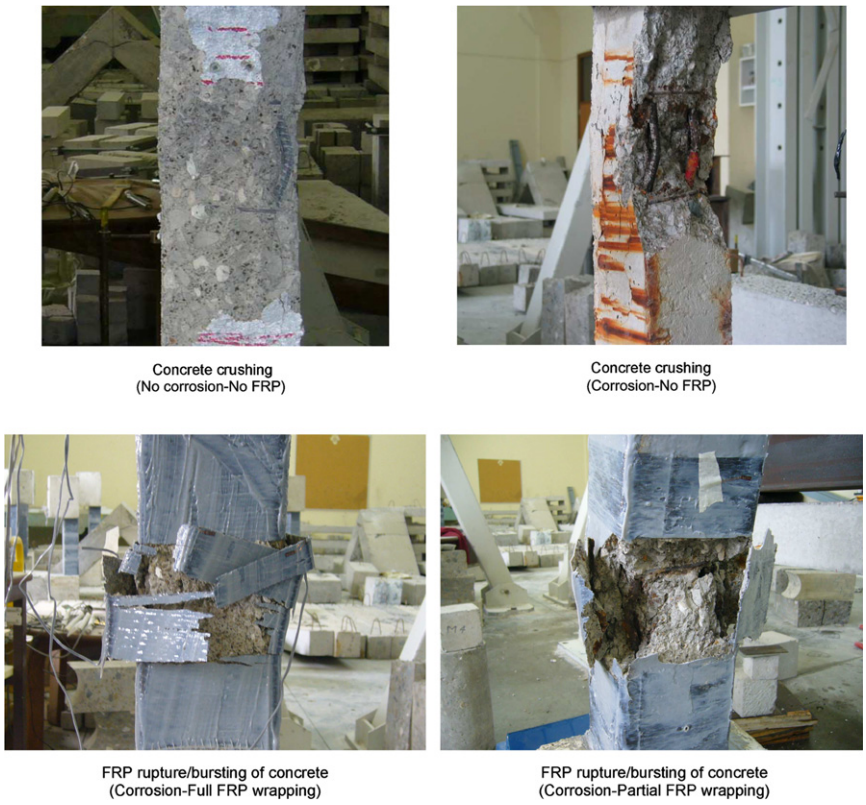

Fig. 10. Various failure modes.

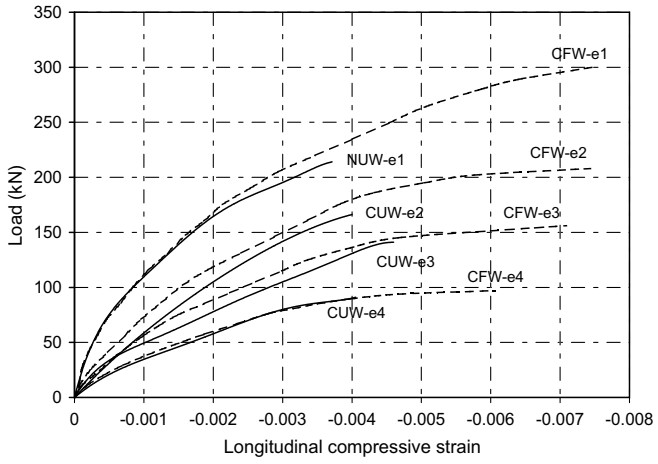

Fig. 11. Load–longitudinal compressive strain relationship.

realistic material constitutive laws and accounts for the confinement effect of the CFRP on the columns' strength.

4.1. Material modeling

The stress–strain relationship of an unconfined concrete in compression is described by a parabolic relationship [18] (see Fig. 12a).

$$f_c = f'_c\left[\frac{2\varepsilon_c}{\varepsilon_{co}} - \left(\frac{\varepsilon_c}{\varepsilon_{co}}\right)^2\right] \quad (1)$$

with:

$$\varepsilon_{co} = \frac{2f'_c}{E_c} \quad (2)$$

and a concrete Young's modulus of [19]:

$$E_c = 4500\sqrt{f'_c}\ \text{MPa} \quad (3)$$

where f_c is the concrete stress, ε_c the concrete strain, f'_c the concrete compressive strength, ε_{co} the concrete strain corresponding to a concrete compressive strength f'_c, and E_c the concrete Young's modulus in MPa. The lateral confinement provided by the ties is neglected.

The stress–strain model of CFRP-confined concrete is divided into two portions (see Fig. 12b). The proposed model assumes that the first ascending branch of the curve, between zero stress and a stress equal to f'_c, is parabolic similar to that of the unconfined concrete [20,21]. Beyond f'_c, the concrete stress is assumed to increase linearly until it reaches the confined strength of concrete f'_{cc} [22,23]. The strength and the corresponding ultimate compressive strain of a CFRP-confined concrete, f'_{cc} and ε_{cc}, respectively, are given by [23]:

$$f'_{cc} = f'_c\left(1 + 2.15\frac{f_l}{f'_c}\right) \quad (4)$$

$$\varepsilon_{cc} = \varepsilon_{co}\left(2 + 15\frac{f_l}{f'_c}\right) \quad (5)$$

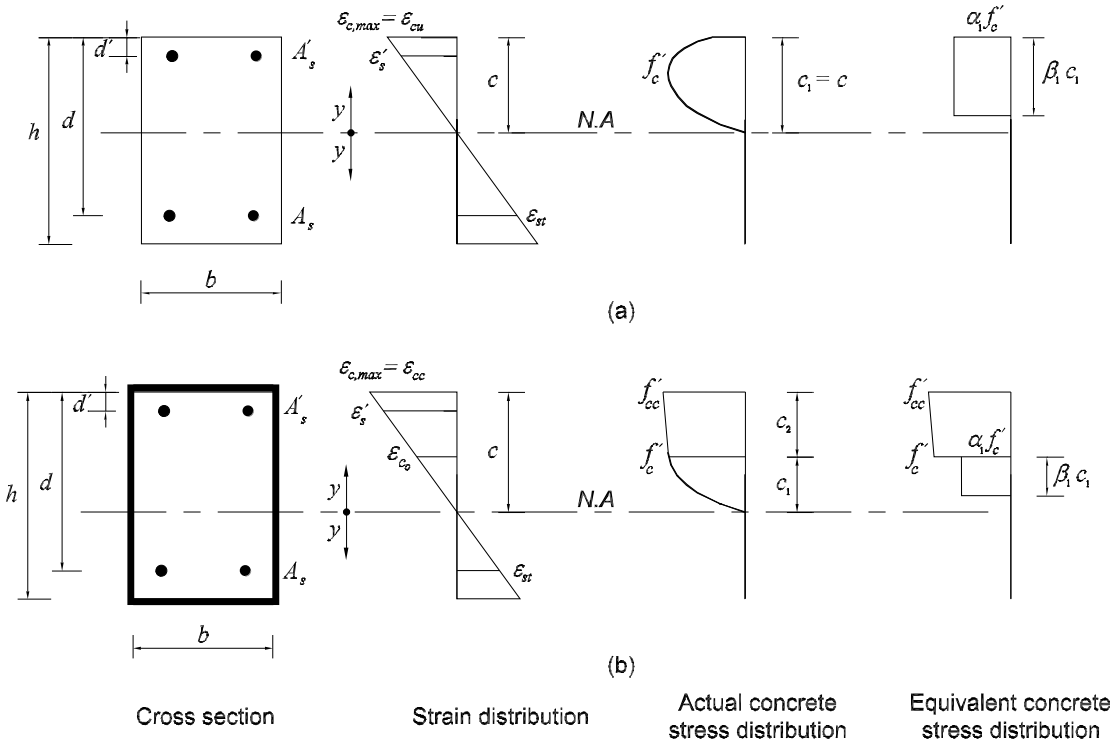

Fig. 12. Strain and stress distribution: (a) unwrapped columns; (b) FRP-wrapped columns.

where f_l is the effective lateral confining pressure provided by CFRP. For a non-circular RC column, the effective lateral confining pressure provided by CFRP-wrapping can be calculated as follows [23,24]:

$$f_l = k_s \frac{2 f_{fr} t_{fe}}{\frac{1}{2}(b+h)} \tag{6}$$

$$t_{fe} = \begin{cases} t_f & \text{full-wrapping} \\ \frac{w_f}{s_f} t_f & \text{partial-wrapping} \end{cases} \tag{7}$$

where k_s is the shape factor that is the ratio of the effective confined area, A_e, to the gross concrete area enclosed by CFRP, A_g, f_{fr} the rupture strength of CFRP, t_{fe} the effective thickness of CFRP, b the section width, h the section depth, t_f is the thickness of one layer of CFRP composite laminate, w_f the width of the CFRP strip in partial-wrapping system, and s_f the center to center spacing between CFRP strips in partial-wrapping system. The shape factor, k_s, can be calculated as follows [13,23]:

$$k_s = \left[1 - \frac{(b-2R_c)^2 + (h-2R_c)^2}{3A_g} - \rho_s\right] \Big/ (1-\rho_s) \tag{8}$$

where R_c is the corner radius, and ρ_s the longitudinal steel ratio.

The stress–strain relationship of steel in tension and compression is idealized to be linear elastic–plastic with a post-yield strain hardening of 1% [25].

$$f_s = \begin{cases} \varepsilon_s E_s & \text{pre-yield stage} \\ f_y + E_{sp}(\varepsilon_s - \varepsilon_{sy}) & \text{post-yield stage} \end{cases} \tag{9}$$

where f_s is the steel stress, ε_s the steel strain, E_s the steel modulus in pre-yield stage, f_y the steel yield strength, E_{sp} the steel modulus in post-yield stage, and ε_{sy} the steel yield strain.

4.2. Strain compatibility and equilibrium condition

The strain and stress distributions over the section depth for unwrapped and CFRP-wrapped columns are shown in Fig. 12a and b, respectively. The strains in the compression and tension steel, ε'_s and ε_{st}, respectively at failure are given by:

$$\varepsilon'_s = \frac{\varepsilon_{c,\max}(c-d')}{c} \tag{10}$$

$$\varepsilon_{st} = \frac{\varepsilon_{c,\max}(d-c)}{c} \tag{11}$$

where $\varepsilon_{c,max}$ is the concrete strain at the extreme compression fiber, and c the depth of neutral axis, d' the depth of compression steel, and d the depth of tension steel. At failure, $\varepsilon_{c,\max} = \varepsilon_{cu}$ for an unconfined concrete while for a CFRP-confined concrete $\varepsilon_{c,\max} = \varepsilon_{cc}$. The value of ε_{cc} is given by Eq. (5) while ε_{cu}, the ultimate compressive strain of an unconfined concrete, is assumed to be 0.0038 [26,27]. For a column section with a constant width the parabolic portion of concrete stress distribution can be replaced by an equivalent rectangular block introducing the stress

block factors α_1 and β_1 [18]. The resultant force of the equivalent rectangular block have the same magnitude and location as those of the actual parabolic stress distribution.

$$\alpha_1 = \left[\frac{\varepsilon_{cp}}{\varepsilon_{co}} - \frac{1}{3}\left(\frac{\varepsilon_{cp}}{\varepsilon_{co}}\right)^2\right] \Big/ \beta_1 \tag{12}$$

$$\beta_1 = \frac{4 - \varepsilon_{cp}/\varepsilon_{co}}{6 - 2\varepsilon_{cp}/\varepsilon_{co}} \tag{13}$$

where ε_{cp} is the concrete strain at the end of the parabolic portion of the concrete stress distribution. At failure, $\varepsilon_{cp} = \varepsilon_{cu}$ for unwrapped columns while for CFRP-wrapped columns $\varepsilon_{cp} = \varepsilon_{co}$.

At failure, equilibrium conditions are imposed in terms of axial force, P_n, and bending moment, M_n.

$$\alpha_1\beta_1 f'_c c_1 b + \frac{f'_{cc} + f'_c}{2} c_2 b + A'_{so}\left(1 - \frac{m_l}{100}\right) f'_s - A_{so}\left(1 - \frac{m_l}{100}\right) f_{st} = P_n \tag{14}$$

$$\left(\alpha_1\beta_1 f'_c c_1 b + \frac{f'_{cc} + f'_c}{2} c_2 b\right)\left(\frac{h}{2} - d_c\right) + A'_{so}\left(1 - \frac{m_l}{100}\right) f'_s\left(\frac{h}{2} - d'\right) + A_{so}\left(1 - \frac{m_l}{100}\right) f_{st}\left(d - \frac{h}{2}\right) = M_n \tag{15}$$

with

$$d_c = c - \frac{(\alpha_1\beta_1 f'_c c_1)(c_1 - \frac{\beta_1 c_1}{2}) + (\frac{f'_{cc} + f'_c}{2} c_2)(c_1 + \frac{2f'_{cc} + f'_c}{3(f'_{cc} + f'_c)} c_2)}{\alpha_1\beta_1 f'_c c_1 + \frac{f'_{cc} + f'_c}{2} c_2} \tag{16}$$

$$c_1 = \begin{cases} c & \text{unwrapped columns} \\ c\left(\frac{\varepsilon_{co}}{\varepsilon_{cc}}\right) & \text{CFRP-wrapped columns} \end{cases} \tag{17}$$

$$c_2 = \begin{cases} 0 & \text{unwrapped columns} \\ c\left(1 - \frac{\varepsilon_{co}}{\varepsilon_{cc}}\right) & \text{CFRP-wrapped columns} \end{cases} \tag{18}$$

where c_1 is the height of the parabolic portion of the concrete stress distribution, c_2 the height of the trapezoidal portion of the concrete stress distribution, d_c the distance between the extreme compression fiber and the resultant compression force in concrete, A'_{so} the original area of compression steel, f'_s the stress in compression steel, A_{so} the original area of tension steel, f_{st} the stress in tension steel, and m_l the steel mass loss (%).

4.3. Model procedure

The model procedure used to predict the column strength can be summarized as follows:

- For a given external eccentricity (e_{ext}), assume depth of the neutral axis (c).
- Calculate compression and tension steel strains that satisfy compatibility requirements.
- Calculate the nominal compression force (P_n) and bending moment (M_n) that satisfy equilibrium requirements.
- Calculate the internal eccentricity ($e_{int} = \frac{M_n}{P_n}$) and compare it to the external value (e_{ext}).
- By trial and error revise the assumed neutral axis depth (c) until $e_{ext} = e_{int}$.
- Record the nominal compression and bending strengths (P_n and M_n, respectively).

Table 3
Model verification

Group	Specimen	Experimental strength (kN)	Predicted strength (kN)	Error (%)[a]
[A]	NUW-e1	215	222.82	+3.6
	NUW-e2	165	170.25	+3.2
	NUW-e3	145	138.90	−4.2
	NUW-e4	92	86.79	−5.7
[B]	CUW-e2	167	171.39	+2.6
	CUW-e3	141	138.11	−2.0
	CUW-e4	91	84.93	−6.7
[C]	CFW-e1	300	279.40	−6.9
	CFW-e2	208	211.96	+1.9
	CFW-e3	156	152.71	−2.1
	CFW-e4	97	91.88	−5.3
[D]	CPW-e1	276	268.23	−2.8
	CPW-e2	203	208.84	+2.9
	CPW-e3	153	150.48	−1.6
	CPW-e4	94	91.09	−3.1

[a] Error (%) = 100 × (predicted − experimental)/(experimental).

4.4. Model verification

The proposed model was utilized to predict the strength of all specimens. Sectional geometry, material properties, and actual eccentricity ratios reported earlier were used as input data in the analysis. The predicted and experimental compression strengths with the percent error between them are given in Table 3. From this table it is evident that all predicted results are within 7% error band. This confirms the ability of the proposed model to accurately predict the compression strength of both unwrapped and CFRP-wrapped RC columns at various eccentric loading.

5. Conclusions

The effectiveness of using CFRP-wrapping system to upgrade corrosion-damaged RC columns under combined flexural and axial loading is examined in this paper. Based on the research results, the following conclusions can be drawn:

- 4.25% steel mass loss that corresponded to an average corrosion crack width of about 0.4 ± 0.12 mm had no noticeable effect on the load carrying capacity of eccentrically loaded RC columns.

- The strengths of the damaged columns fully wrapped with CFRP were 40% and 26% higher than those of the control undamaged columns at nominal e/h values of 0.3 and 0.43, respectively. The strength gain was less pronounced at higher eccentricity ratios. Only 8% and 5% enhancements in the load carrying capacity were recorded at nominal e/h values of 0.57 and 0.86, respectively.
- At nominal e/h value of 0.3, the strength of the corrosion-damaged specimen repaired with partial CFRP-wrapping was about 8% lower than that of its counterpart repaired with full CFRP-wrapping. No significant variation in strength was observed at higher e/h values.
- An analytical model that can predict the strength of eccentrically loaded RC columns wrapped with CFRP was proposed and verified against test results.

Acknowledgements

The author would like to express his appreciation to the Research Affairs at the UAE-University for the financial support of this project under fund Grant # 03-01-7-11/07. The author would like to thank the Undergraduate Research Assistants and the Laboratory Specialists at the UAE-University for their help throughout testing.

References

[1] Andrade C, Alonso C, Molina FJ. Cover cracking as a function of bar corrosion: Part I – Experimental test. Mater Struct 1993;26:453–64.
[2] Clark LA, Saifullah M. Effect of corrosion on reinforcement bond strength. In: International conference on structural faults and repair; 1993. p. 113–9.
[3] Rodriguez J, Ortega LM, Garcia AM. Assessment of structural elements with corroded reinforcement. In: Swamy ED, Sheffield RN, editors. Corrosion and corrosion protection of steel in concrete. Sheffield: Academic Press; 1994. p. 171–85.
[4] Bonacci JF, Maalej M. Externally bonded fiber-reinforced polymer for rehabilitation of corrosion damaged concrete beams. ACI Struct J 2000;97(5):703–11.
[5] El Maaddawy TA, Soudki KA. Carbon-fiber-reinforced polymer repair to extend service life of corroded reinforced concrete beams. ASCE J Compos Construct 2005;9(2):187–94.
[6] El Maaddawy TA, Soudki KA, Topper T. Performance evaluation of carbon fiber reinforced polymer – repaired beams under corrosive environmental conditions. ACI Struct J 2007;104(1):3–11.
[7] Lee C, Bonacci J, Thomas M, Maalej M, Khajehpour S, Hearn N, et al. Accelerated corrosion and repair of reinforced concrete columns using fibre reinforced polymer sheets. Can J Civil Eng 2000;27(5):941–8.
[8] Pantazopoulou S, Bonacci J, Sheikh S, Thomas M, Hearn N. Repair of corrosion-damaged columns with FRP wraps. ASCE J Compos Construct 2001;5(1):3–11.
[9] Debaiky A, Green M, Hope B. Carbon fiber-reinforced polymer wraps for corrosion control and rehabilitation of reinforced concrete columns. ACI Mater J 2002;99(2):129–37.
[10] Ma R, Xiao Y. Seismic retrofit and repair of circular bridge columns with advanced composite materials. Earthquake Spectra 1999;15(4):747–64.
[11] Anggawidjaja D, Ueda T, Dai J, Nakai H. Deformation capacity of RC piers wrapped by new fiber-reinforced polymer with large fracture strain. Cement Concr Compos 2006;28(10):914–27.
[12] Iacobucci R, Sheikh S, Bayrak O. Retrofit of square concrete columns with carbon fiber-reinforced polymers for seismic resistance. ACI Struct J 2003;100(6):78594.
[13] Chaallal O, Shahawy M. Performance of fiber-reinforced polymer-wrapped reinforced concrete column under combined axial-flexural loading. ACI Struct J 2000;97(4):659–69.
[14] Parvin A, Wang W. Behavior of FRP jacketed concrete columns under eccentric loading. Journal of Composites for Construction, ASCE 2001;5(3):146–52.
[15] Hadi M. Behaviour of FRP wrapped normal strength concrete columns under eccentric loading. J Compos Struct 2006;74:503–11.
[16] ASTM International. Standard practice for preparing, cleaning, and evaluating corrosion test specimens, ASTM G1-90; 2002.
[17] Féderation International du Béton (fip Bulletin). Bond of reinforcement in concrete, state-of-art report. Bulletin No. 10; 2000. Switzerland: International Federation for Structural Concrete. p. 188–215.
[18] Collins MP, Mitchell D. Prestressed concrete basics; 1987. Ottawa, ON, Canada: Canadian Prestressed Concrete Institute (CPCI).
[19] Canadian Standards Association (CSA) A23.3-94. Design of concrete structures; 1994. Rexadle, ON, Canada: Canadian Standards Association.
[20] Samaan M, Mirmiran A, Shahawy M. Models of concrete confined by fiber composite. J Struct Eng, ASCE 1998;124(9):1025–31.
[21] Fam A, Flisak B, Rizkalla S. Experimental and analytical modeling of concrete-filled fiber-reinforced polymer tubes subjected to combined bending and axial loads. ACI Struct J 2003;100(4):499–509.
[22] Mirmiran A, Shahawy M, Samaan M. Strength and ductility of hybird FRP-concrete beam-columns. J Struct Eng, ASCE 1999;125(10):1085–93.
[23] Teng J, Chen J, Smith S, Lam L. FRP-strengthened RC structures. England: John Wiley & Sons Ltd.; 2002.
[24] Cusson D, Paultre P. Stress–strain model for confined high-strength concrete. J Struct Eng, ASCE 1995;121(3):468–77.
[25] El Maaddawy TA, Soudki KA, Topper T. Computer-based mathematical model for performance prediction of corroded beams repaired with fiber reinforced polymers. J Compos Construct, ASCE 2005;9(3):227–35.
[26] Park R, Paulay T. Reinforced concrete structures. NY, USA: John Wiley and Sons.
[27] El Maaddawy TA, Soudki KA, Topper T. Analytical model to predict the non-linear flexural behavior of corroded reinforced concrete beams. ACI Struct J 2005;102(4):550–9.